Journal of Catalysis **205,** 44–57 (2002)
doi:10.1006/jcat.2001.3426, available online at http://www.idealibrary.com on IDEAL®

Genesis of Brønsted Acid Sites during Dehydration of 2-Butanol on Tungsten Oxide Catalysts

Chelsey D. Baertsch, Kenny T. Komala, Yong-Hwee Chua, and Enrique Iglesia[1]

Department of Chemical Engineering, University of California at Berkeley, Berkeley, California 94720

Received March 29, 2001; revised September 9, 2001; accepted September 9, 2001

In situ **measurements of Brønsted acid sites (by titration with 2,6-di-*tert*-butyl-pyridine) and reduced centers (by UV–vis spectroscopy) were carried out on WO_x–ZrO_2 with catalysts at 2.9–32.3 W/nm^2 in order to probe how these species form and act as active sites during 2-butanol dehydration. The rate of 2-butanol dehydration (per W-atom) on WO_x–ZrO_2 reached maximum values at intermediate WO_x surface densities, as was also found previously for *o*-xylene and *n*-pentane isomerization. Polytungstate domains prevalent at these surface densities balance the accessibility of W^{6+} centers with their ability to reduce to form Brønsted acid sites via reduction with 2-butanol. *In situ* UV–vis spectra showed that 2-butanol reduces WO_x species and that the highest density of the Brønsted acid sites formed is obtained at WO_x surface densities similar to those required for maximum dehydration rates. Brønsted acid site densities were measured during 2-butanol reaction using sterically hindered 2,6-di-*tert*-butyl-pyridine, which titrates only Brønsted acid sites. 2-Butanol dehydration requires Brønsted acid sites that form during reaction at low concentrations (0.040 sites/W-atom) and reach their highest concentration at intermediate WO_x surface densities (6.8–14.8 W/nm^2). Pre-edge features in UV–vis spectra are weak for monotungstate species (<4 W/nm^2) and their intensity increase is parallel to that observed in 2-butanol dehydration rates, confirming the requirement for active $H^{\delta+}(WO_3)_n^{\delta-}$ species, formed during reaction and stabilized by polytungstate domains. Turnover rates (per Brønsted acid site) are much higher on WO_x–ZrO_2 than on Lewis acid sites active for 2-butanol dehydration on γ-Al_2O_3. 2-Butanol dehydration turnover rates (per Brønsted acid site) on SiO_2-supported tungstophosphoric acid (HPW), however, are higher than those on WO_x–ZrO_2. The mechanism-based rate equation developed for 2-butanol dehydration and the faster secondary butene isomerization found on HPW suggest that acid sites are weaker on HPW than on WO_x–ZrO_2. A weaker acidity is indeed expected from the stronger conjugate base provided by the smaller WO_x domains and the larger H^+/W ratio in HPW clusters. Weaker acid sites allow faster product desorption and higher turnover rates from saturated surfaces during 2-butanol dehydration.**

Key Words: **Brønsted acid site density; catalytic titration; UV–vis spectroscopy; alcohol dehydration mechanism.**

INTRODUCTION

Inorganic solid acids based on tungsten oxide nanostructures supported on zirconia have received significant attention since Hino and Arata (1) first showed that WO_x–ZrO_2 (15 wt% W) catalyzed the isomerization of *n*-butane and *n*-pentane at ~300 K after treatment in air at high temperatures (1073–1123 K). Structural characterization using Raman, UV–vis, and X-ray absorption spectroscopies showed that two-dimensional polytungstate species at near-monolayer coverages (~8 W-atoms/nm^2) lead to maximum isomerization rates (2–4). These studies also showed that the WO_x surface densities (W-atoms/nm^2), and not the W content or the treatment temperature independently, control the structure, domain size, and catalytic properties of active WO_x species. Polytungstate species appear to provide the balance between the reducibility and accessibility of WO_x centers required for high Brønsted acid site densities.

Kinetic and mechanistic studies of *o*-xylene isomerization in the presence of H_2 showed that catalytic rates are proportional to the H_2 concentration in the reactant stream and to the amount of H_2 chemisorbed during reaction (3, 5, 6). This promotional effect of H_2 is related to the formation of $H^{\delta+}(WO_3)_n^{\delta-}$ Brønsted acid sites via the local reduction of polytungstate domains, without the removal of lattice oxygen atoms. These sites catalyze isomerization and dehydration reactions much more effectively than acidic OH groups in W–O–W and W–O–Zr species (3, 5, 6) or in H–ZSM5 (6, 7). Recently, the redox processes that lead to the concurrent formation of reduced W centers and Brønsted acid sites were also detected during *n*-pentane isomerization using electron spin resonance and infrared spectroscopic methods (8).

Isomerization and dehydration reaction rates are low on monotungstate species prevalent at submonolayer WO_x coverages and on WO_3 crystallites present at high surface coverages. Above monolayer WO_x coverages, the formation of WO_3 crystallites leads to inaccessible WO_x and to the formation of oxygen-deficient WO_{3-x} species at typical reaction conditions (4, 5). WO_{3-x} species appear to

[1] To whom correspondence should be addressed. Fax: 510-642-4778. E-mail: iglesia@cchem.berkeley.edu.

0021-9517/02 $35.00

provide stronger conjugate bases than stoichiometric WO_3 and do not delocalize the electron density required to stabilize $H^{\delta+}$ species formed from H_2 as effectively as WO_3. At low WO_x coverages, the prevalent species are isolated monotungstate species, which are difficult to reduce (3, 9, 10); they do not form $H^{\delta+}$ acid centers via dissociation of H–H, C–H or O–H bonds in H_2, alkane, or alcohol reactants.

Several studies have explored the strong effects of WO_x structure on catalytic properties by probing the density and type of acid sites in WO_x–ZrO_2 as a function of the synthesis procedures used. Infrared spectroscopy of adsorbed pyridine (11, 12), ammonia (5, 7), and CO (at 80 K) (13) has shown that WO_x–ZrO_2 catalysts contain both Brønsted and Lewis acid sites. The ratio of Brønsted to Lewis acid sites is low at submonolayer WO_x coverages, but increases with increasing surface density. These data suggest that Brønsted acid sites require bridging W–O–W species, such as those present in polytungstate species.

These characterization methods, however, probe site densities under conditions (temperature, pressure, surface coverage) far removed from catalytic reaction conditions. As a result, these methods detect only permanent Brønsted acid sites and not the "temporary" $H^{\delta+}(WO_3)_n^{\delta-}$ species that appear to form in the presence of H_2 or other reductants. The marked effects of these reductants on reaction rates suggest that such $H^{\delta+}(WO_3)_n^{\delta-}$ species account for the high isomerization rates obtained on polytungstate domains. A very low density of Brønsted acid sites on near-monolayer WO_x–ZrO_2 was previously reported ($\sim$0.0024 H^+/W-atom) by titrating Brønsted acid sites with 2,6-dimethyl-pyridine during *n*-pentane isomerization (14). Isotopic exchange using D_2 and H_2 chemisorption measurements under typical reaction conditions (523 K, $\sim$1 bar H_2) gave site densities of 0.020 and 0.031 H^+/W-atom, respectively (5). NH_3 adsorption measurements (at 298 K) gave much higher acid site densities (0.15–0.20 Brønsted acid sites/W-atom), because NH_3 also titrates "permanent" Brønsted and Lewis acid sites (5) with much lower catalytic activity. Clearly, characterization methods that measure the density of Brønsted acid sites present under typical reaction conditions and formed in reducing atmosphers are required in order to accurately measure the number of $H^{\delta+}(WO_{3-x})^{\delta-}$ redox sites.

Here, we use 2-butanol dehydration as a probe reaction in order to explore the acid and redox properties of WO_x–ZrO_2 catalysts with varying WO_x surface densities and the number and type of sites required for dehydration reactions. In contrast with more complex alkane isomerization reactions, alcohol reactions do not require an additional nonacidic function in order to complete a turnover. We report the use of *in situ* chemical titration methods to measure Brønsted and Lewis acid site densities by adding 2,6-di-*tert*-butyl-pyridine or pyridine titrants during 2-butanol dehydration reactions. We also address the mechanism of 2-butanol dehydration and its Brønsted acid site requirements and clarify some inconsistencies in previous literature treatments of alcohol dehydration reactions. Finally, we examine the redox properties of WO_x centers and their role in Brønsted acidity by using *in situ* UV–vis spectroscopic measurements of the extent and rate of the reduction processes that occur during 2-butanol dehydration reactions on WO_x-based acid catalysts.

EXPERIMENTAL

Catalyst Preparation

WO_x–ZrO_2 catalysts were prepared by aqueous impregnation of zirconium oxyhydroxide with a tungsten salt, using previously reported procedures (1, 15). Zirconium oxyhydroxide ($ZrO_x(OH)_{4-2x}$) was precipitated from a 0.5 M aqueous solution of zirconyl chloride ($ZrOCl_2 \cdot 8H_2O$, Aldrich, >98 wt%) at a constant pH of 10 using NH_4OH. The precipitate was filtered and washed in order to remove residual Cl^- ions and then dried at 383 K. The resulting $ZrO_x(OH)_{4-2x}$ was impregnated to incipient wetness with aqueous ammonium metatungstate solutions ($(NH_4)_6H_2W_{12}O_{40}$, Strem Chemicals, 99.9%) containing the desired amount of W, dried at 383 K, and then treated in flowing dry air (Matheson, zero grade, 0.50 $cm^3\ s^{-1}$) at 773–1173 K. WO_3 concentrations of 15 or 30 wt% led to a wide range of WO_x surface densities (2.9–29.8 W-atoms/nm^2) after thermal treatment in dry air at 773–1173 K.

Silica-supported 12-tungstophosphoric acid (HPW) was prepared by incipient wetness impregnation of SiO_2 (Davidson 62) with a 40 wt% $H_3PW_{12}O_{40} \cdot 6H_2O$ (Baker) aqueous solution. The resulting HPW/SiO_2 was dried at 393 K and then treated in ambient air at 573 K. The BET surface area of this sample was 161 m^2/g. The alumina used was γ-Al_2O_3 (Engelhard, reforming grade) with a BET surface area of 158 m^2/g.

The W content, treatment temperature, BET surface area, and calculated surface density for each sample are reported in Table 1. Multipoint BET isotherms were obtained on all samples from N_2 physisorption uptakes at its normal boiling point using a Quantasorb surface area analyzer after evacuating samples at 473 K for 4 h.

Catalytic Reactions of 2-Butanol

The catalytic dehydration of 2-butanol (Aldrich, 99.5%, anhydrous) was carried out at 343–403 K in a quartz flow reactor ($\sim$1.0-cm i.d.) containing $\sim$0.030 g of 120–250 μm catalyst pellets dispersed on a quartz frit. Samples were treated in flowing dry air (0.83 $cm^3\ s^{-1}$) at 773 K for WO_x–ZrO_2 (2.9–32.3 W/nm^2), 723 K for γ-Al_2O_3, and 523 K for HPW/SiO_2 before catalytic reaction measurements. Liquid 2-butanol (Aldrich, 99.5%, anhydrous) was introduced into flowing He or H_2 (Mattson, UHP) at 1 bar and $\sim$373 K using a syringe pump to control the 2-butanol concentration

TABLE 1

WO_x–ZrO_2 Properties and Nomenclature

W concentration (wt% WO_3)	Treatment temperature (K)	Surface area (m^2/g)	Surface density (W/nm^2)	Nomenclature
30	773	200	3.9	$W_{30}Z$-3.9
30	873	144	5.4	$W_{30}Z$-5.4
30	923	115	6.8	$W_{30}Z$-6.8
30	973	81	9.6	$W_{30}Z$-9.6
30	1023	52	14.8	$W_{30}Z$-14.8
30	1073	45	17.2	$W_{30}Z$-17.2
30	1123	24	32.3	$W_{30}Z$-32.3
15	873	132	2.9	$W_{15}Z$-2.9
15	1023	49	7.9	$W_{15}Z$-7.9
15	1073	40	10.5	$W_{15}Z$-10.5
15	1123	29	13.5	$W_{15}Z$-13.5
15	1173	13	29.8	$W_{15}Z$-29.8

(0.25–1.00% mol). The conversion of 2-butanol was varied by changing the carrier flow rate (0.15–5.78 cm^3 s^{-1}) at a constant 2-butanol pressure; the resulting space velocities are reported as υ/ω, where υ is the carrier flow rate in cubic centimeters per second and ω is the number of W g-atoms in the catalyst sample. H_2O was introduced in some experiments as a liquid mixture with 2-butanol (1 : 1 molar ratio). Reactant and product concentrations were measured by gas chromatography (Hewlett–Packard 6890 GC, 30-m HP-1 capillary column, flame ionization detector). The rates of 2-butanol dehydration are reported as W-atom turnover rates (moles of 2-butanol converted per g-atom W per second), unless otherwise noted.

Titration of Acid Sites during 2-Butanol Dehydration Reactions

Liquid mixtures of 2-butanol with pyridine (Fischer, 99.9%) or with 2,6-di-*tert*-butyl-pyridine (Aldrich, 97%) were prepared by mixing 4.5 ml of 2-butanol (Aldrich, 99.5%, anhydrous) with 20 μl of either organic base. The resulting reactant mixture was introduced into a He stream (1.33 cm^3 s^{-1}) at a liquid volumetric flow rate of 0.09 cm^3 h^{-1}, resulting in mole fractions of 5×10^{-3} for 2-butanol, 2.5×10^{-5} for pyridine, or 9.0×10^{-6} for 2,6-di-*tert*-butylpyridine. The amount of titrant adsorbed on the catalyst was estimated from its concentration in the reactant and effluent streams, measured by gas chromatography.

UV–Visible Diffuse Reflectance Spectroscopy

Diffuse reflectance spectra of finely ground WO_x–ZrO_2 samples (~0.150 g) were obtained in the ultraviolet–visible (UV–vis) range using a Varian (Cary 4) spectrometer with a Harrick Scientific diffuse reflectance attachment (DRP-XXX) and a controlled environment reaction chamber (DRA-2CR). Reflectance measurements were converted into absorbance units using the Kubelka–Munk function and MgO as a perfect reflector reference (3).

Temperature-programmed reduction studies were carried out in the UV–vis cell using either H_2 (101.3 kPa, 1.33 cm^3 s^{-1}) or 2-butanol (0.5 mol%) in He (1.33 cm^3 s^{-1}) as reductants. The samples were dehydrated in flowing dry air at 723 K, cooled to 298 K, treated in He at 298 K, and then exposed to the reductant at 298 K, while measuring UV–vis spectra after each treatment. The sample temperature was then gradually increased at 0.083 K s^{-1}, and spectra were obtained at ~25 K increments. The observed weak effects of temperature on the UV–vis absorbance were taken into account by subtracting spectra obtained at similar temperatures, but in the absence of a reductant (pure He, 1.33 cm^3 s^{-1}). The reduction processes that occurred during steady-state reaction of 0.5 mol% 2-butanol in He (1.33 cm^3 s^{-1}) at 323 K were monitored by UV–vis measurements as a function of time in contact with the reactant stream.

RESULTS AND DISCUSSION

Catalytic Reactions of 2-Butanol

The dehydration of 2-butanol was used in order to probe the acid properties and the *in situ* formation of acid sites in WO_x–ZrO_2 catalysts on samples with a wide range of WO_x surface density. Dehydration rate and acid site titration measurements were also carried out on γ-Al_2O_3, which contains predominantly Lewis acid sites, and on a WO_x-based solid acid with "permanent" Brønsted acidity (SiO_2-supported 12-tungstophosphoric acid). Only dehydration products were detected (1-butene, *cis*- and *trans*-2-butenes) in the temperature range examined (343–403 K). In general, bimolecular dehydration reactions of secondary or tertiary alcohols leading to ethers are very slow compared to monomolecular pathways leading to alkenes (16, 17), especially at low alcohol concentrations.

Figure 1 shows steady-state 2-butanol dehydration rates on $W_{30}Z$-3.9, $W_{30}Z$-9.6, and $W_{30}Z$-17.2 at 373 K as a function of time on stream. As reported for other acid-catalyzed

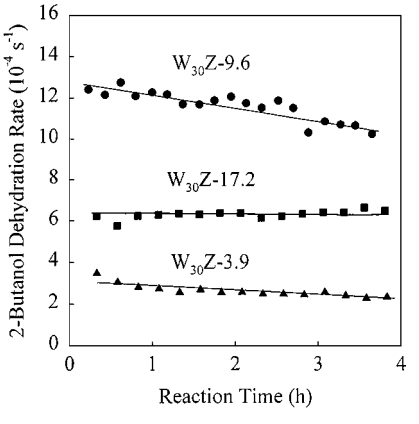

FIG. 1. 2-Butanol dehydration rate (per W-atom) at 373 K as a function of time on stream and WO_x surface density (3.9, 9.6, and 17.2 W/nm^2) (0.5 kPa 2-butanol, 100.8 kPa He, 19–33% initial conversion).

reactions (4, 14, 18), initial 2-butanol dehydration rates are strongly influenced by the WO_x surface density. $W_{30}Z$-9.6 shows the highest dehydration rate among these WO_x–ZrO_2 catalysts. This sample contains the highest density of polytungstate species and it also showed maximum rates for *o*-xylene isomerization (4). Deactivation was slow or negligible on all WO_x–ZrO_2 samples (Fig. 1).

2-Butanol conversion was not detectable on γ-Al_2O_3 at 373 K, but near-complete conversion was achieved on HPW/SiO_2; thus, reaction temperatures of 403 and 343 K were required to compare dehydration rates on WO_x–ZrO_2 catalysts to those on γ-Al_2O_3 and HPW/SiO_2, respectively. A detailed comparison of γ-Al_2O_3 HPW/SiO_2, and WO_x–ZrO_2 catalysts will be presented later; but these initial measurements at 373 K clearly show that specific rates (per gram) decreased in the order HPW/SiO_2 > WO_x–ZrO_2 > γ-Al_2O_3.

Dehydration rates were measured on all WO_x–ZrO_2 samples at 373 K (Table 1, 2.9–29.8 W/nn^2) as a function of 2-butanol conversion (1–50%), which was varied by changing the space velocity during steady-state reactions. On all WO_x–ZrO_2 samples, dehydration rates decreased with increasing conversion, as shown in Fig. 2 for $W_{30}Z$-6.8. This appears to reflect a kinetic inhibition of dehydration rates by one of the reaction products. Rigorous comparisons of 2-butanol dehydration rates on WO_x–ZrO_2 as a function of WO_x surface density must therefore be made at similar 2-butanol conversion levels, preferably using reaction rate constants for a mechanism-based rate expression. Such expressions allow rigorous comparisons of kinetic rate constants. The favorable thermodynamics for 2-butanol dehydration (100% conversion at 373 K) and the conversion range within which inhibition was first detected led us to discard reverse reaction rates as the cause of the lower dehydration rates observed as conversion increased.

The depletion of the 2-butanol reactant with increasing conversion is not sufficient to account for the lower rates

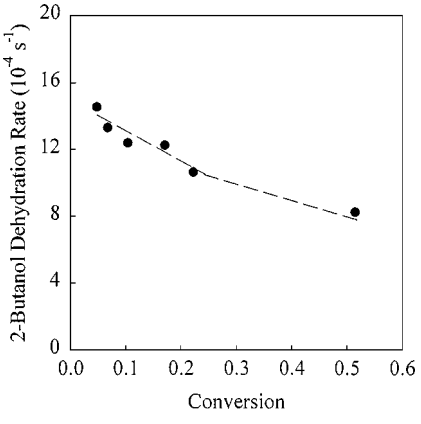

FIG. 2. 2-Butanol dehydration rate (per W-atom) at 373 K as a function of conversion for $W_{30}Z$-6.8 (0.5 kPa 2-butanol, 100.8 kPa He, 11–219 mol 2-butanol/g-atom W-h).

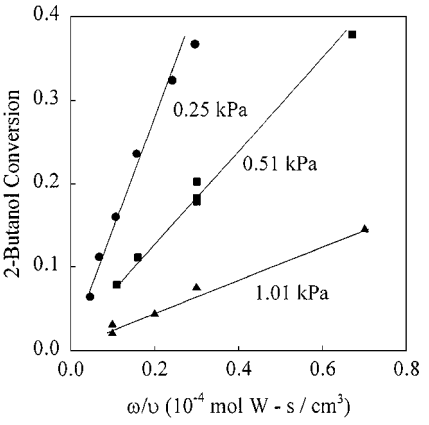

FIG. 3. 2-Butanol conversion at 373 K as a function of residence time and 2-butanol concentration (indicated in figure) for $W_{30}Z$-9.6. (ω/υ = inverse space velocity, where ω = g-atoms W in sample and υ = He flow rate in cm^3 s^{-1}.)

as conversion increases, which occurs even at very low 2-butanol conversions (<10%). In Fig. 3, 2-butanol conversions are shown as a function of residence time on $W_{30}Z$–9.6 at 373 K for three different 2-butanol concentrations (0.25, 0.51, and 1.01 kPa). At a given residence time, the conversion is higher at lower 2-butanol concentrations, suggesting a zero-order dependence on alcohol concentration. First-order 2-butanol kinetics would have led to concentration-independent conversions, in the absence of product inhibition effects. The zero-order rate constants shown in Table 2 were estimated from the data in Fig. 3, using least-squares error minimization procedures and a well-mixed reactor model appropriate for the thin catalyst bed used. There is a small, but detectable decrease in the apparent zero-order rate constant as the 2-butanol concentration in the feed increases. This appears to reflect the inhibition of dehydration rates by H_2O, a reaction product that becomes more prevalent (at a given conversion) as the 2-butanol reactant concentration increases.

The inhibition by H_2O was confirmed by adding H_2O (0.5 kPa) during reactions of 2-butanol (0.5 kPa) on $W_{30}Z$-9.6. Figure 4 shows the conversion of 2-butanol as a function of space velocity with and without H_2O added. At all conversions, the addition of 0.5 kPa H_2O decreased dehydration rates to $\sim 8 \times 10^{-4}$ s^{-1}, a value that is lower than

TABLE 2

Zero-Order Rate Constants for 2-Butanol Dehydration at 373 K on $W_{30}Z$-9.6[a]

2-Butanol concentration (kPa)	Zero-order rate constant (10^{-4} s^{-1})
0.25	14.6
0.50	13.9
1.01	12.0

[a] Obtained from analysis of the data in Fig. 3.

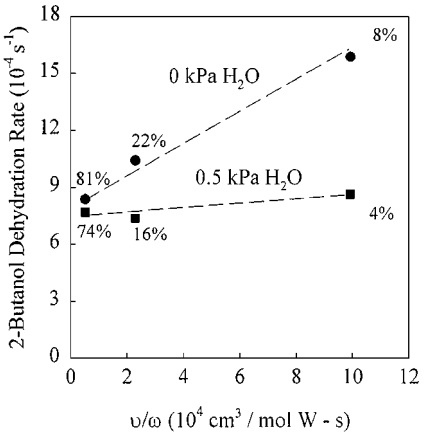

FIG. 4. 2-Butanol dehydration rate (per W-atom) at 373 K as a function of space velocity for $W_{30}Z$-9.6 (●) (0.5 kPa 2-butanol). The effect of adding 0.5 kPa H_2O to the feed is also shown (■). Conversion is reported in the figure for each data point.

the rate measured without added water at all but the highest 2-butanol conversion. The rate in the presence of 0.5 kPa added H_2O is similar to that obtained in the experiment at 81% conversion using pure 2-butanol as the reactant, during which 0.4 kPa H_2O forms (Fig. 4). These inhibition effects appear to arise from competitive adsorption of H_2O and 2-butanol on active sites. Saturation coverages of H_2O appear to occur near 0.4 kPa, at which point rates decreased to a low constant value at all conversions (Fig. 4). At the conversions used in this study (<50%), H_2O pressures are less than 0.25 kPa, and 2-butanol dehydration rates show an inverse dependence on the pressure of the H_2O formed by the reaction (Fig. 2). Thus, as long as the H_2O pressure is below saturation levels (~0.4 kPa), dehydration rates are inversely proportional to the H_2O concentration generated *in situ*.

Figure 5 shows the selectivity to butene isomers as a function of WO_x surface density (2.9–32.3 W/nm^2). These selectivities are reported at ~5% conversion, but selectivities

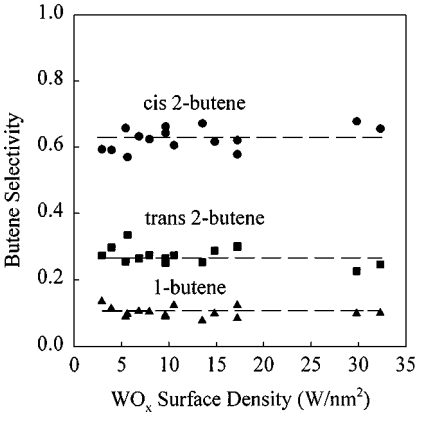

FIG. 5. Butene selectivity at 373 K as a function of WO_x surface density at ~5% conversion (0.5 kPa 2-butanol, 100.8 kPa He).

were not influenced by 2-butanol conversion in the conversion range covered (1–50%). Significant changes in the number and nature (Lewis vs Brønsted) of the acid sites have been observed with changes in WO_x surface density (7). Yet, 2-butanol dehydration selectivities were not affected by these structural changes, suggesting either that only one type of acid site (Brønsted or Lewis) catalyzes these dehydration reactions or that any different types of sites present lead to identical selectivities. The average values of the selectivities to butene isomers (from Fig. 5) were 63% *cis*-2-butene, 27% *trans*-2-butene, and 10% 1-butene. This product selectivity differs markedly from the expected equilibrium distribution (26.4% *cis*-2-butene; 66.7% *trans*-2-butene; 6.8% 1-butene) (19), and it remains constant over a wide range of 2-butanol conversion, suggesting that alkenes form as primary products and that secondary butene isomerization steps do not occur. Butenes do not readsorb and undergo double-bond isomerization after desorption, and dehydration steps lead directly to the formation of all detected isomers during one surface sojourn. Larsen *et al.* (20) previously concluded that alkene readsorption did not occur during reactions with 2-propanol on WO_x–ZrO_2. They did not detect the incorporation of D-atoms into the propene formed from CH_3–HCOD–CH_3, which would have occurred if propene readsorbed on D^+ Brønsted acid sites (formed by rapid exchange of OH groups with the labeled alcohol) (20).

The preferential formation of *cis*-2-butene in butanol dehydration reactions has been previously reported (at low conversions) on both Lewis and Brønsted acid catalysts, including Al_2O_3 (16, 17), WO_3 (21), and SiO_2–Al_2O_3 (22). Early alcohol dehydration studies suggested that on Al_2O_3, dehydration of primary, secondary, and even tertiary alcohols occurs via concerted E-2-type pathways at low temperatures (<473 K) (Shown in Scheme 2). These pathways involve the concerted elimination of the OH and β-hydrogen in the alcohol on electron acceptor–donor pair sites, consisting of either a cation (Lewis acid) or a proton (Brønsted acid) bonded to a lattice oxygen atom (23). This concerted mechanism was confirmed by the large kinetic isotope effects measured for alcohols with D-atoms at β-positions (23). Kinetic isotope effects would have been very small for E-1-type dehydration mechanisms, for which the rate is controlled by the loss of OH groups to form carbenium ions that form alkenes via subsequent β-hydrogen elimination.

In order to form *cis*-alkene products during E-2 elimination, transition states must adapt a synclinal conformation, as shown in Scheme 1a for a secondary alcohol. Steric interactions between the adsorbed alcohol and the catalyst surface appear to be more important than the intramolecular steric constraints present in the required conformation (Scheme 1a), which is less energetically favorable than the configuration shown in Scheme 1b, because of the close proximity of the CH_3 and R-alkyl substituents.

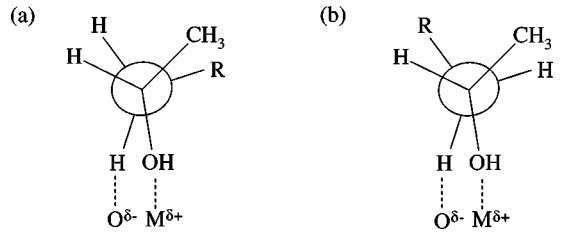

SCHEME 1. E-2 dehydration transition state conformations required for the formation of *cis*-alkenes (a) and *trans*-alkenes (b).

Previous studies using Al_2O_3 showed that bulkier R groups (in Scheme 1) decreased *cis*-alkene selectivities; therefore, increased intramolecular steric constraints are required for transition states with *trans* configuration (24).

The selective formation of *cis*-alkenes may indeed arise from an E-2-type mechanism, but equilibrium alkene distributions (selective formation of *trans*-alkenes) do not necessarily show that E-1-type pathways are involved. Yet, several studies have proposed this, arguing that free rotation in the carbenium ions involved in E-1 pathways is required for equilibrium alkene distributions during a dehydration event (25). A product distribution that reflects the stability of molecules in the gas phase can only be achieved via multiple surface sojourns and not merely by free rotation of carbenium ion intermediates. The thermodynamics of adsorbed (and not gas-phase) species determine the relative abundance of the various adsorbed precursors as well as their desorption rates; these will not, in general, reflect the thermodynamic stability of the gas-phase alkenes formed from these adsorbed precursors. Thermodynamic *cis–trans* equilibrium is approached only via secondary isomerization reactions; alkene isomerization tends to occur rapidly on unoccupied Brønsted acid sites and slowly, if at all, on Lewis acid sites or on Brønsted acid sites with a high coverage of alcohol-derived intermediates. Equilibrated *cis–trans* alkene products reflect the presence of Brønsted acid sites, which are required for isomerization. However, the preferred formation of *cis*-alkenes can also occur on Brønsted acid sites, as long as secondary isomerization reactions do not occur. For example, if alkenes compete unsuccessfully for active sites with alcohol-derived reactive intermediates, or if the residence time of the alkenes formed is short, the high *cis* selectivity of the primary dehydration pathway is maintained. Equilibrium alkene distributions are favored at high temperatures, because unoccupied sites become available for alkene adsorption, or in the constrained geometries within zeolite channels, where diffusional restrictions increase the residence time and the readsorption probability of alkenes.

On WO_x–ZrO_2 catalysts, high *cis*-2-butene selectivities are observed over a wide range of conversion (1–50%), and secondary isomerization reactions are not detected. 2-Butanol dehydration is catalyzed predominantly by Brønsted acid sites on WO_x–ZrO_2, as shown later, but high coverages of butanol-derived intermediates inhibit olefin readsorption and secondary isomerization. These butanol-derived intermediates are the most abundant adsorbed species, as shown by the near-zero-order kinetics of the 2-butanol dehydration reaction. The reaction mechanism for 2-butanol dehydration shown in Scheme 2 is consistent with the kinetic dependence on 2-butanol and H_2O concentrations, and with the absence of secondary butene isomerization events; it is not intended to represent the different stereochemical conformations.

These elementary steps include the reversible nondissociative adsorption of 2-butanol on active sites (step 1), which consist of conjugate acid–base pairs interacting in a concerted manner with the OH group and one α-hydrogen in 2-butanol (Scheme 2). These active sites consist of a cation ($M^{\delta+}$) and a lattice oxygen anion ($O^{\delta-}$), where the cation is $H^{\delta+}$ for a Brønsted acid site, such as those responsible for the reaction on WO_x–ZrO_2. The adsorption of 2-butanol is followed by a concerted (E-2) decomposition to form butene isomers and two vicinal OH groups. When $M^{\delta+}$ is a Lewis acid center, H_2O desorbs via recombination of these hydroxyl groups (step 3a), re-forming the metal–oxygen bond that was cleaved during step 2. When the cation is a proton ($H^{\delta+}$), hydronium ions form during alcohol decomposition (step 2), and then desorb to re-form the Brønsted acid site (step 3b).

The reversibility of step 3 is consistent with the observed H_2O inhibition effects. The addition of *trans*-2-butene (1 kPa) did not influence 2-butanol dehydration

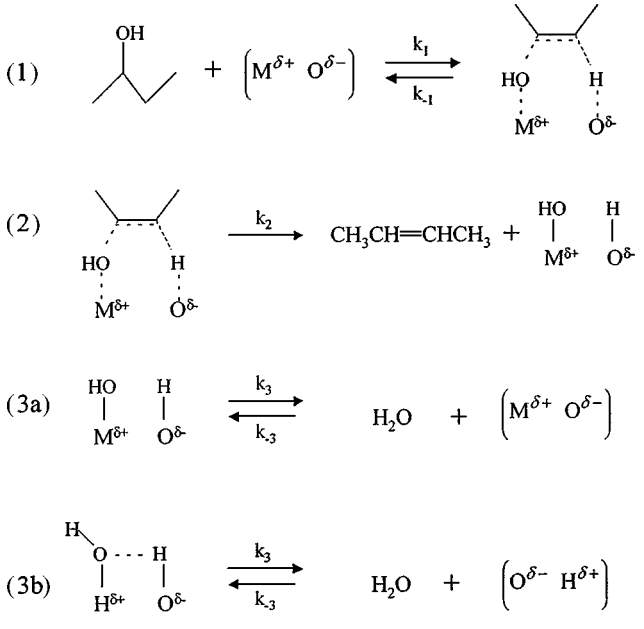

SCHEME 2. Proposed elementary steps for 2-butanol dehydration on WO_x–ZrO_2 catalysts. Pathways of H_2O desorption from Lewis acid sites and from Brønsted acid sites are compared in steps 3a and 3b, respectively.

rates, suggesting that step 2 is irreversible. The application of the pseudo-steady-state assumption for all intermediates in Scheme 1 leads to

$$r = \frac{k_2 k_1 [A][L]}{(k_{-1} + k_2)\left(1 + \frac{k_{-3}}{k_3}[H_2O] + \frac{k_1(1 + k_2/k_3)[A]}{(k_{-1} + k_2)}\right)}, \quad [1]$$

where $[L]$ is the total concentration of active sites, $[A]$ is the 2-butanol concentration, and $[H_2O]$ is the water concentration. When the concentration of unoccupied sites is much smaller than that of adsorbed species, this equation reduces to

$$r = \frac{\left(\frac{k_2[L]}{1 + k_2/k_3}\right)}{\left(1 + \frac{k_{-3}(k_{-1} + k_2)}{k_3 k_1 (1 + k_2/k_3)} \frac{[H_2O]}{[A]}\right)} = \frac{k'}{1 + \alpha \frac{[H_2O]}{[A]}} \approx \frac{k'}{1 + \beta[H_2O]}. \quad [2]$$

At low conversions, the concentration of 2-butanol is very similar to the inlet value and much greater than the water concentration, leading to the observed near-zero-order kinetic dependence on the 2-butanol concentration and to the weak observed inhibition by H_2O.

Experimental rates were extrapolated to zero reactant conversion using Eq. [2] in order to obtain initial dehydration rates, which reflect apparent zero-order rate constants ($k' = k_2/[1 + k_2/k_3]$). These initial rates are shown in Fig. 6 as a function of WO_x surface density. As in the case of *o*-xylene isomerization (4, 15), 2-butanol dehydration rates depend on the WO_x surface density, irrespective of whether it is achieved by changing the W content or the treatment temperature. Low 2-butanol dehydration rates (per W-atom) were obtained at low surface densities (<4 W/nm^2) on samples containing predominantly monotungstate species (4, 15). As isolated WO_x species condense into polytungstate species with increasing surface density (4, 15), 2-butanol dehydration rates increase; they reach a maximum value at surface densities similar to those required to form a polytungstate monolayer (~7–8 W/nm^2). At higher surface densities, dehydration rates decrease to an almost constant value (~4×10^{-4} s^{-1}) as three-dimensional WO_3 crystallites form.

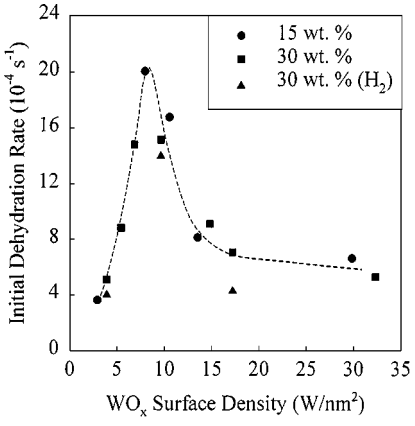

FIG. 6. Initial 2-butanol dehydration rate (per W-atom) at 373 K as a function of WO_x surface density. Two tungsten concentrations are shown (WO_3 basis), 15 wt% (●) and 30 wt% (■), using He (100.8 kPa) as the carrier. The 30 wt% sample is also shown using H_2 (100.8 kPa) as the carrier (▲).

The marked effects of the WO_x domain size on the rate of acid-catalyzed reactions (Fig. 6) reflect an increase in the reducibility of WO_x domains with increasing size (4, 9, 14). *In situ* UV–vis spectroscopy and reduction kinetic studies showed that the rate and extent of reduction of WO_x increased with increasing domain size (3, 9, 10). H_2 is required for high *o*-xylene isomerization rates on WO_x–ZrO_2 at 523 K, because it leads to the stoichiometric formation of reduced $H^{\delta+}$-$W^{(6-\delta)+}O_3$ centers in polytungstate domains. The acidic $H^{\delta+}$ species formed by reaction with H_2 are stabilized by electron delocalization over WO_x domains, without loss of lattice oxygens to form inactive WO_{3-x} species (6, 7). The formation of Brønsted acid sites via such redox processes was previously detected on Pt-promoted SO_x–ZrO_2 (26) and on Ag and Cu salts of 12-tungstophosphoric acid (27). The effects of WO_x surface density on 2-butanol dehydration rates indicate that a similar mechanism may be involved in the formation of the Brønsted acid sites required for this reaction.

The addition of H_2 (100 kPa) during 2-butanol dehydration at 373 K, however, did not influence 2-butanol dehydration rates (Fig. 6, triangles) at any WO_x surface density. H_2 chemisorption studies on WO_x–ZrO_2 have shown that H_2 activation requires temperatures of ~500 K (5). Therefore, H_2 would not be expected to form Brønsted acid sites at 373 K. These findings, however, leave unanswered the question of whether Brønsted acid sites are indeed required for 2-butanol reactions, and if they are, how they form at 373 K without the involvement of H_2.

Early studies of ethanol dehydration on WO_3 powders showed that WO_3 reduces to $WO_{2.5}$ at ~523 K during an induction period within which dehydration rates increase (28). Thus, it is possible that 2-butanol also reduces smaller supported WO_x domains at ~373 K. Below, we show that Brønsted acid sites are required for 2-butanol dehydration turnovers by adding a selective titrant for Brønsted acid sites during 2-butanol dehydration reactions. We also report UV–vis spectroscopic data *during* 2-butanol dehydration, which show that reduced centers indeed form during the catalytic reaction. The number of these reduced centers increases with increasing WO_x surface density and correlates with the 2-butanol dehydration rates obtained on each sample.

Titration of Acid Sites during 2-Butanol Dehydration Reactions

The continuous addition of a basic titrant during 2-butanol dehydration was used to measure the density and

type of acid sites present in WO_x–ZrO_2 required for 2-butanol dehydration. Pyridine coordinates with W^{6+} Lewis centers and it is also protonated by Brønsted acid sites; thus, it measures the total number of acid sites. In contrast, the bulky groups near the nitrogen atom in 2,6-di-*tert*-butyl-pyridine prevent its coordination to Lewis acid centers, but not protonation, as reported previously for less hindered 2,6-di-methyl-pyridine (14, 29).

2,6-Di-*tert*-butyl-pyridine did not adsorb or influence 2-butanol dehydration rates at 403 K on γ-Al_2O_3, which lacks Brønsted acidity and catalyzes dehydration reactions using only Lewis acid sites. These experiments confirmed that 2,6-di-*tert*-butyl-pyridine does not titrate Lewis acid sites or even adsorb competitively with 2-butanol on γ-Al_2O_3 at 403 K. The addition of pyridine, however, decreased 2-butanol dehydration rates on γ-Al_2O_3, confirming that pyridine titrates the available Lewis acid sites. Even after saturation of γ-Al_2O_3 surfaces with pyridine, 2-butanol dehydration rates remained at ~50% of the initial value. This may reflect the competitive adsorption of pyridine and 2-butanol on Lewis acid sites that are too weak to adsorb pyridine irreversibly. Thus, the density of active sites measured from titration measurements using pyridine at 403 K on γ-Al_2O_3 may underestimate the number of Lewis acid sites involved in 2-butanol dehydration turnovers.

Figure 7 shows 2-butanol dehydration rates at 373 K on W_{30}Z-14.8 as a function of the cumulative amount of titrant adsorbed (pyridine or 2,6-di-*tert*-butyl-pyridine). Figure 7 shows that 2-butanol dehydration on W_{30}Z-14.8 requires only Brønsted acid sites, because rates decreased to very low values (<1% of initial rate; $\sim 0.06 \times 10^{-4}$ s^{-1}) after saturation with 2,6-di-*tert*-butyl-pyridine. Pyridine also titrates the required Brønsted acid sites, but the amount required to inhibit rates is higher than that for 2,6-di-*tert*-butyl-pyridine, because complete titration of both Brønsted and Lewis acid sites is required before the titrant reaches active Brønsted acid sites near the exit of the catalyst bed. The total density of acid sites (Brønsted and Lewis) on W_{30}Z-14.8 is 0.055 sites/W-atom and is obtained from the *x*-intercept of the pyridine titration data shown in Fig. 7. The Brønsted acid site density obtained from 2,6-di-*tert*-butyl-pyridine titration data is 0.035 sites/W-atom. The difference between these two values (0.020 sites/W-atom) reflects the density of Lewis acid sites available during reaction. Dehydration rates decreased proportionately with the amount of 2,6-di-*tert*-butyl-pyridine adsorbed (Fig. 7), suggesting that dehydration turnover rates are similar on all Brønsted acid sites present in W_{30}Z-14.8. These experiments do not rule out, however, the presence of a nonuniform distribution of site activities, because these data were obtained by adding the titrant to a sample bed of finite depth, such that adsorption occurs on the first available binding site, irrespective of acid strength. This unavoidable difficulty also means that it is possible that some of the Brønsted acid sites that bind 2,6-di-*tert*-butyl-pyridine strongly at 373 K do not catalyze 2-butanol dehydration; thus, the acid site densities measured represent an upper limit to the number of active centers.

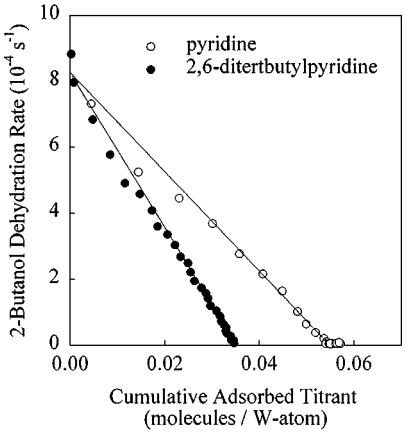

FIG. 7. Catalytic titration of W_{30}Z-14.8: 2-butanol dehydration rate at 373 K (per W-atom) as a function of the cumulative amount of titrant (2,6-di-*tert*-butyl-pyridine or pyridine) adsorbed during reaction (0.5 kPa 2-butanol, 100.1 kPa He).

The results of titration measurements during 2-butanol dehydration on WO_x–ZrO_2 samples with a wide range of WO_x surface density (W_{30}Z-3.9, W_{30}Z-6.8, W_{30}Z-9.6, W_{30}Z-14.8, and W_{30}Z-17.2) are shown in Fig. 8 as Brønsted (a) and Lewis (b) acid site densities. Figure 8a shows that WO_x–ZrO_2 catalysts with intermediate WO_x surface densities (6.8, 9.6, and 14.8 W/nm^2), corresponding to 1–2 equiv polytungstate monolayers, lead to the highest Brønsted acid site densities (0.035–0.040/W-atom). Samples with 6.8 and 9.6 W/nm^2 also gave the highest 2-butanol dehydration rates (Fig. 6), as expected from the active nature of such Brønsted acid sites in 2-butanol dehydration reactions on WO_x–ZrO_2 and from the ability of adsorbed 2,6-di-*tert*-butyl-pyridine to titrate, selectively and irreversibly, such Brønsted acid sites. The density of active Brønsted acid sites is very low, and ~25 W-atom ensembles appear to be required, on average, in order to stabilize one H^+ site.

Brønsted acid site densities remained high for W_{30}Z-14.8, even though 2-butanol dehydration rates decreased significantly from the maximum values obtained on samples with near monolayer WO_x coverages (Fig. 6). At a surface density of 14.8 W/nm^2, WO_x domains have aggregated into WO_3 crystallites, which can form H_xWO_3 bronzes during 2-butanol reactions at 373 K. In such samples, 2,6-di-*tert*-butyl-pyridine may also be able to titrate protonic sites in the bulk bronze, because protons can segregate to the surface after surface OH groups are titrated by the organic base. As a result, the number of accessible protons may exceed those present at the bronze surfaces. At a surface density corresponding to ~3 WO_x monolayers (17.2 W/nm^2), the Brønsted acid site density decreased markedly to ~0.025 sites/W-atom. At this high surface

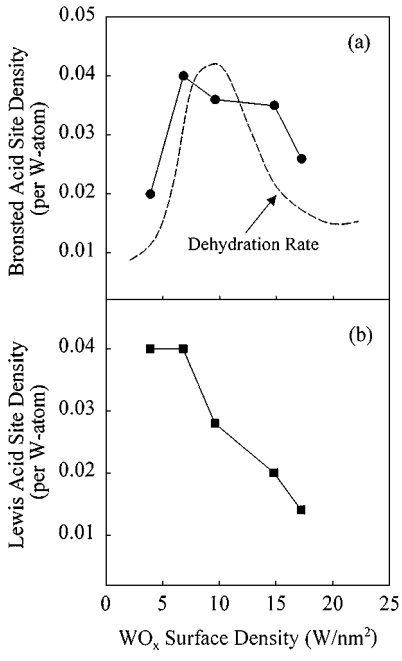

FIG. 8. Acid site density [Brønsted (a) and Lewis (b)] as a function of WO_x surface density. Acid site densities were determined by titration during 2-butanol reaction at 373 K with pyridine (Brønsted + Lewis acid site density) or 2,6-di-*tert*-butyl-pyridine (Brønsted acid site density).

density, reduction can lead to significant removal of lattice oxygens (5); these reduced $W^{(6-\delta)+}$ centers cannot stabilize surface H^+ species by delocalizing additional electrons.

The density of Lewis acid sites (Fig. 8b) is highest (~0.040 sites/W-atom) on WO_x–ZrO_2 samples with submonolayer WO_x coverages (W_{30}Z-3.9 and W_{30}Z-6.8). W^{6+} cations become inaccessible as three-dimensional WO_3 clusters form, and the number of Lewis acid sites (per W) decreases monotonically as the WO_x surface density increases (Fig. 8b). The residual 2-butanol dehydration rates measured after 2,6-di-*tert*-butyl-pyridine saturation suggest that Lewis acid sites on WO_x–ZrO_2 contribute slightly to the measured steady-state dehydration rates (Table 3). This contribution decreases as the density of accessible Lewis acid sites decreases with increasing WO_x surface density (Fig. 8b). After complete titration with pyridine, 2-butanol dehydration rates are very low ($\sim 0.08 \times 10^{-4}$ s^{-1}) on all WO_x–ZrO_2 samples and resemble the lowest values obtained after saturating Brønsted acid sites with 2,6-di-*tert*-butyl-pyridine (0.06×10^{-4} s^{-1}, from Table 3). These data suggest that steady-state rates may contain a very small but detectable contribution either from basic sites present on ZrO_2 at a similar low value in all WO_x–ZrO_2 samples or from acid sites that are incompletely saturated by either titrant, because of competitive adsorption of 2-butanol reactants, during reactions at 373 K.

TABLE 3

Residual 2-Butanol Dehydration Rates on Lewis Acid Sites after Titration with 2,6-Di-*tert*-butyl-pyridine

Catalyst	2-Butanol dehydration rate on Lewis acid sites (10^{-4} s^{-1})
W_{30}Z-3.9	0.47
W_{30}Z-6.8	0.32
W_{30}Z-9.6	0.25
W_{30}Z-14.8	0.06
W_{30}Z-17.2	0.08

The amount of 2,6-di-methyl-pyridine required to inhibit *n*-pentane isomerization is also very low on WO_x–ZrO_2 (15 wt% W; ~6.3 W/nm^2) (14). These measurements involved a complex treatment procedure, which attempted to measure only strong acid sites, and a catalytic reaction that requires bifunctional pathways and dehydrogenation initiation steps (30, 31). 2,6-Di-methyl-pyridine was preadsorbed before reaction. The samples were then treated in flowing N_2 at 573 K for 13 h in an effort to redistribute the titrant onto the strongest Brønsted acid sites. The rate of *n*-pentane isomerization was then measured, and the Brønsted acid site density was reported to be 0.0024 H^+/W-atom. The nonlinear correlation of *n*-pentane isomerization rate with the amount of 2,6-di-methyl-pyridine adsorbed suggested the presence of less active weaker Brønsted acid sites and led to a total Brønsted acid site density of 0.0114 H^+/W-atom. These site densities are much smaller than those reported in the present study (0.040 H^+/W-atom) on samples with similar WO_x surface densities (W_{30}Z-6.8). This may reflect differences in procedures, since our titration measurements may include Brønsted acid sites that are inactive for 2-butanol dehydration, such as OH sites at W–O–W and W–O–Zr interfaces, resulting in artificially high site densities. The acid strength requirements for these two reactions are also different. Pentane isomerization requires either very strong Brønsted acid sites or bifunctional reaction pathways involving dehydrogenation sites in addition to Brønsted acid sites. The total density of these redox sites may not have been accurately measured, because H_2 is required to form these active sites; but it was not present during 2,6-dimethyl-pyridine adsorption and pretreatment. In any case, Brønsted acid site densities are low in WO_x–ZrO_2; these sites form via reduction processes and require extended WO_x domains.

The density of acid sites in WO_x–ZrO_2 polytungstate domains and their 2-butanol dehydration turnover rates were compared to those in silica-supported 12-tungstophosphoric acid (HPW/SiO_2). 2,6-Di-*tert*-butyl-pyridine adsorption during 2-butanol dehydration at 343 K led to complete inhibition at uptakes of 0.185 H^+/W-atom (2.22 $H^+/PW_{12}O_{40}^{3-}$ Keggin cluster). This value is

slightly smaller than that expected from the stoichiometry of the Keggin cluster (0.25 H^+/W). This may reflect the incomplete accessibility of internal protons in the ~5 nm $H_3PW_{12}O_{40}$ crystallites present on SiO_2, or the dehydroxylation of some Keggin clusters during thermal pretreatment at 573 K. A total (Brønsted + Lewis) site density of 0.275 H^+/W-atom (3.30 $H^+/PW_{12}O_{40}$) was measured from the pyridine uptake. This suggests that dehydroxylation may have led to the replacement of protons with acidic W^{6+} centers attached to O atoms bridging 2 Keggin units. As also observed on WO_x–ZrO_2 catalysts, these Lewis acid sites did not contribute significantly to steady-state 2-butanol dehydration rates.

These titration measurements allow a comparison of 2-butanol dehydration turnover rates (per Brønsted acid site) on WO_x–ZrO_2 to those on HPW/SiO_2 as well as to those (per Lewis acid site) on γ-Al_2O_3. Table 4 compares 2-butanol dehydration rates on W_{30}Z-6.8 and γ-Al_2O_3 at 403 K and on W_{30}Z-9.6 and HPW/SiO_2 at 343 K. The two WO_x–ZrO_2 catalysts used in this comparison (W_{30}Z-9.6 and W_{30}Z-6.8) showed very similar 2-butanol dehydration rates (Fig. 6) and Brønsted acid site densities (Fig. 8a). The marked differences in turnover rates for γ-Al_2O_3 and HPW/SiO_2 prevented the comparison of all samples at the same temperature. Rates are reported on the basis of catalyst mass, BET surface area, number of W-atoms, or number of acid sites (Brønsted or Lewis). Dehydration turnover rates were highest on HPW/SiO_2 and lowest on γ-Al_2O_3. Turnover rates on WO_x–ZrO_2 at 403 K were ~70 times greater than those on γ-Al_2O_3, reflecting the much higher activity of Brønsted acid sites compared to that of Lewis acid sites present on γ-Al_2O_3.

TABLE 4

Comparison of 2-Butanol Dehydration Rates on WO_x–ZrO_2, Alumina, and 12-Tungstophosphoric acid

Catalyst	W_{30}Z-9.6	γ-Al_2O_3	W_{30}Z-6.8	HPW/SiO_2
Reaction temperature (K)	403	403	343	343
Conversion (%)	34	15	23	25
Dehydration rates ($\times 10^3$)				
Per g catalyst[a]	1.67	0.0112	0.00517	0.320
Per area[b]	168.0	0.577	0.366	16.2
Per W-atom[c]	17.50	N/A	0.0539	2.69
Per acid site[d]	486.0[e]	7.47[f]	1.35[e]	14.6[g]

[a] g 2-butanol converted/g catalyst/s.
[b] Molecules 2-butanol converted/nm^2 surface area/s.
[c] Molecules 2-butanol converted/W-atom/s.
[d] Molecules 2-butanol converted/acid site/s.
[e] Per Brønsted acid site, determined from 2,6-di-*tert*-butyl-pyridine titration at 373 K.
[f] Per Lewis acid site, determined from pyridine titration at 403 K.
[g] Per Brønsted acid site, determined from 2,6-di-*tert*-butyl-pyridine titration at 343 K.

2-Butanol dehydration turnover rates were ~10 times higher on HPW/SiO_2 than on WO_x–ZrO_2. This may appear surprising at first, because the $(PW_{12}O_{40})^{3-}$ clusters stabilizing 3 H^+ in HPA catalysts are more electron rich, and therefore they are stronger conjugate bases than the WO_x domains stabilizing a small number of protons (0.035 H^+/W-atom) on WO_x–ZrO_2 samples. Butene distributions confirmed the weaker acidity of protons in the HPA sample. The distribution of butenes on HPW/SiO_2 (47% *cis*-2-butene, 47% *trans*-2-butene, 6% 1-butene; 3% conversion) was closer to equilibrium values than that on WO_x–ZrO_2, and approached equilibrium with increasing conversion. This reflects the availability of unoccupied Brønsted acid sites for secondary isomerization reactions, because of the weaker binding of adsorbed intermediates derived from 2-butanol and H_2O on HPW/SiO_2 than that on WO_x–ZrO_2. The weaker acidity of the heteropolyacid protons is consistent with the weaker H_2O inhibition observed on HPW/SiO_2 compared to WO_x–ZrO_2. At low conversions, the concentration of water-derived intermediates is very low, such that

$$\left[\frac{k_{-3}(k_{-1}+k_2)}{k_3k_1(1+k_2/k_3)}\frac{[H_2O]}{[A]}\right] \ll 1$$

in Eq. [2], which then becomes

$$r = \frac{1}{\frac{1}{k_2}+\frac{1}{k_3}}. \qquad [3]$$

Thus, an increase in either k_2 or k_3 as acid sites become weaker would increase 2-butanol dehydration rates. Weaker acid sites in HPW/SiO_2 compared to WO_x–ZrO_2 may account for the higher dehydration rates obtained on HPW/SiO_2. The differences in turnover rates on these two W-based catalysts may also reflect, in part, an overestimate of the density of $H^{\delta+}$-$W^{(6-\delta)+}O_3$ sites in WO_x–ZrO_2, because 2,6-di-*tert*-butyl-pyridine can also irreversibly titrate (at 373 K) OH groups at W–O–W and W–O–Zr sites, which are not required for 2-butanol reactions. These findings provide a useful, and probably common, example of acid-catalyzed reactions for which weaker acid sites lead to faster turnovers.

UV–Visible Spectroscopy Studies

In this section, we examine the role of WO_x surface density on 2-butanol dehydration rates and on WO_x reduction processes in order to reconcile the beneficial effects of the higher reducibility of WO_x domains with the lack of H_2 effects on reaction rates. In the previous section, we showed that 2-butanol dehydration occurs on Brønsted acid sites, which required the presence of H_2 for *o*-xylene isomerization at 523 K (15). Both *o*-xylene isomerization (in the presence of H_2) (15) and 2-butanol dehydration (without H_2;

Fig. 6) reached maximum rates at intermediate WO_x surface densities. In this section, we describe the mechanism by which Brønsted acid sites form *during* 2-butanol dehydration using UV–vis spectroscopy during reaction.

UV–vis spectroscopy was previously used to examine the electronic properties of WO_x–ZrO_2 samples (2, 3), which depend on local coordination and domain size. The absorption edge arises from ligand-to-metal electron transitions, which depend on domain size because confinement within small domains decreases the density of discrete energy levels (32, 33). Here, we exploit absorption features that emerge in the pre-edge energy region as a result of reduced "color centers," which form when electrons are injected into stoichiometric oxides. Discrete d–d electron transitions in transition-metal complexes lead to absorption features in the pre-edge region (34). These d–d transitions are spin-forbidden in such complexes, but weak absorption features become detectable because of orbital degeneracy caused by spin–orbit coupling and Jahn–Teller effects (34). Small semiconductor domains, such as those in WO_x–ZrO_2, act as a species intermediate between bulk and molecular structures and contain a distribution of unoccupied (d-orbital) energy levels within the valence band. Color centers in WO_x domains form via electron donation caused by either removal of lattice oxygens or via reduction by hydrogen to form $W^{(6-\delta)+}$ and $H^{\delta+}$. These electrons are delocalized over discrete semiconducting domains and electronic transitions occur from photon absorption in the visible region. Molecule-like sharp transitions occur for very small domains because of the discrete energy levels available. With increasing domain size, absorption features become broader because of the high density of closely spaced energy levels, which become available by orbital mixing in larger structures.

These reduced centers become detectable on WO_x–ZrO_2 during treatment in H_2 and during reactions of 2-butanol. UV–vis techniques were previously used to monitor the reduction of WO_x–ZrO_2 with H_2 at 523 K (3) and of Mo/SiO_2 with ethanol at 403–513 K (35, 36). Figure 9 shows UV–vis absorption spectra in the pre-edge region (1.5–3.5 eV) during exposure of W_{30}Z-9.6 to 2-butanol (0.5 kPa) at 298–623 K (heating rate 5 K s^{-1}). The incipient reduction of W^{6+} centers was detected below ~373 K, but the pre-edge absorption intensity was very low (Fig. 9), because the transient nature of this measurement led to very short holding times at each temperature. The absorption features became more intense as temperature increased, consistent with the expected increase in the extent of reduction. Weak but distinct features at discrete energies emerged in the pre-edge region (Fig. 9) as a result of electronic transitions within localized "molecule-like" structures. These discrete absorption features appear within a broad absorption background arising from transitions among closely spaced energy levels that become available as semiconductor domains grow.

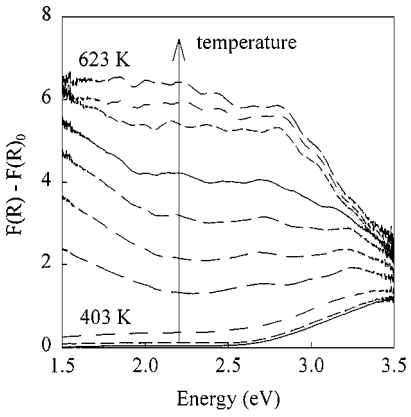

FIG. 9. *In situ* UV–vis absorption spectra in the pre-edge (visible) region for W_{30}Z-9.6 during exposure to 2-butanol (0.5 kPa 2-butanol, 100.8 kPa He) at increasing temperatures. Spectra are shown in increments of ~30° from 298 to 623 K.

These observed absorption features in the UV–vis spectrum do not arise from electronic transitions in adsorbed organic intermediates formed from 2-butanol. The removal of 2-butanol from the gas phase after reaction did not decrease the pre-edge intensity, even after treating in He at 773 K in an attempt to remove any adsorbed species. Therefore, these features in the pre-edge (Fig. 9) reflect only d–d transitions within reduced $W^{(6-\delta)+}$ centers. These pre-edge features disappear after treatment in air at elevated temperatures, which reoxidizes these centers to W^{6+}.

Figure 10 shows the absorption intensity at 2.5 eV as a function of temperature for W_{30}Z-9.6 using 2-butanol (0.5 kPa; from Fig. 9) or H_2 (~100 kPa) as reductants. The pre-edge features are broad; therefore, we chose this energy (2.5 eV) for quantitative comparisons; but other energies in the pre-edge regions led to similar conclusions. Reduced centers were detected in W_{30}Z-9.6 below 350 K using 2-butanol as the reductant. In H_2, similar extents of reduction required temperatures above 500 K, consistent with H_2 chemisorption studies, which showed that H_2 dissociation starts at ~500 K on WO_x–ZrO_2 (5). This is consistent with the ineffectiveness of H_2 in modifying 2-butanol dehydration rates at ~373 K (Fig. 6). The rapid formation of color centers and the concomitant appearance of Brønsted acid sites form by using 2-butanol as a stoichiometric reductant during dehydration reactions. The activation of O–H or C–H bonds in 2-butanol is more facile than the H–H bond activation steps required when H_2 is used as the reductant.

These reduction measurements can be used to estimate the extent of reduction and the density of reduced centers as a function of WO_x surface density, a property of the catalysts that strongly influenced 2-butanol dehydration rates and Brønsted acid site densities. The W_{30}Z-9.6 sample in Fig. 10 contains predominantly two-dimensional polytungstate structures and starts to reduce below 350 K during

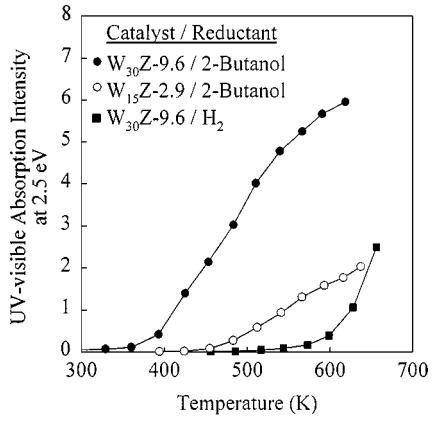

FIG. 10. UV–vis absorption intensity at 2.5 eV as a function of temperature for $W_{30}Z$-9.6 and $W_{15}Z$-2.9 during *in situ* reduction with 2-butanol (0.5 kPa) and for $W_{30}Z$-9.6 during *in situ* reduction with H_2 (100.8 kPa).

2-butanol dehydration reactions. In contrast, reduction in 2-butanol becomes detectable only at ~450 K on $W_{30}Z$-2.9, also shown in Fig. 10, which contains predominantly isolated monotungstate species. As observed with H_2 as the reductant, the reducibility of WO_x domains using 2-butanol increased with increasing WO_x domain size.

Figure 11 shows UV–vis spectra obtained during steady-state 2-butanol dehydration at 323 K (after 1 h) on WO_x–ZrO_2 samples with a wide range of WO_x surface densities. At WO_x surface densities near a polytungstate monolayer ($W_{30}Z$-6.8), samples show a distinct absorption feature at ~2.2 eV. The sharpness of this feature is characteristic of d–d electronic transitions in "molecule-like" structures, such as those expected to be present in very small isolated WO_x domains. The samples with the lowest WO_x surface densities (2.9 and 3.9 W/nm^2) also show this discrete transition, but the intensity of this feature was significantly lower than that in $W_{30}Z$-6.8, because of the less reducible nature of these samples. In the sample with the highest surface density ($W_{30}Z$-17.2), WO_3 crystallites coexist with dispersed structures. This sample showed broad preedge features (1.6–2.9 eV) instead of the discrete absorption bands prevalent at lower WO_x surface densities. Similar broad absorption features, typical of structures that delocalize electrons over closely spaced energy states, were observed during reduction in H_2 at 523 K (3). These reduction processes, which lead to broad features in the UV–vis absorption spectra, appear to involve the removal of some lattice oxygen atoms. The emergence of these absorption features coincides with an increase in the amount of O_2 that adsorbs on WO_x–ZrO_2 samples after reduction in H_2 at 523 K (5). The $W_{30}Z$-9.6 sample shows a mixture of localized and delocalized processes, as expected from coexisting polytungstate domains with $H^{\delta+}$ species and discrete $W^{(6-\delta)+}$ sites, and WO_3 crystallites, which convert to WO_{3-x} during reduction (3–5, 14). The UV–vis edge energy is unchanged (3.1–3.5 eV) by any of these processes, suggesting that these reduction events do not influence the size or coordination of WO_x domains.

The integrated intensity in the pre-edge region (1.5–3.2 eV) during 2-butanol dehydration at 323 K is proportional to the number of electrons stabilized by WO_x domains, either within the band structure of larger domains or in the d-orbitals of "molecule-like" confined structures. These integrated intensities (Fig. 12) increased sharply with increasing domain size at WO_x surface densities similar to those required for the observed marked increases in 2-butanol dehydration rates (Fig. 12, dashed line) and Brønsted acid site densities (Fig. 8a). Dehydration rates, Brønsted acid site densities, and the number of reduced centers showed a strong and parallel dependence on WO_x surface density (Table 5). These data confirm the role of reduced centers in the formation of active Brønsted acid sites and the participation of 2-butanol as the *in situ* reductant during dehydration reactions on WO_x–ZrO_2.

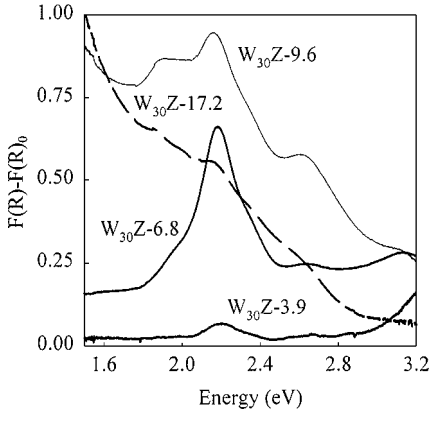

FIG. 11. UV–vis absorption spectra in the pre-edge (visible) region as a function of WO_x surface density during steady-state reaction (after 1 h) with 2-butanol (0.5 kPa) at 323 K.

TABLE 5

Comparison of Acid Site Characterization Parameters as a Function of WO_x Surface Density

Catalyst	Acid site characterization parameter		
WO_x surface density (W/nm^2)	Initial dehydration rate[a] (10^{-4} s^{-1})	Brønsted acid site density[b] (H^+/W-atom)	Relative abundance of reduced centers[c] (a.u.)
3.9	4.4	0.020	0.8
6.8	13.7	0.040	33.1
9.6	13.9	0.036	50.0
17.2	6.4	0.026	32.8

[a] Per W-atom, for 2-butanol dehydration at 373 K.

[b] Determined from titration with 2,6-di-*tert*-butyl-pyridine during reaction with 2-butanol at 373 K.

[c] Relative UV–vis absorption area from 1.5 to 3.2 eV during 2-butanol dehydration at 343 K.

Formation of $H^{\delta+}(WO_3)_n^{\delta-}$ Brønsted Acid/Redox Sites

The formation of Brønsted acid sites can occur by activation of 2-butanol to form H-atoms, which are then stabilized by polytungstate domains, as in the case of H_2 at higher temperatures (3, 5) (Scheme 3). These processes lead to the formation of $H^{\delta+}(WO_3)_n^{\delta-}$ species with acidic OH groups resembling those in H_xWO_3 bronzes. The reduction of WO_x by 2-butanol appears to coincide with the evolution of small amounts of dehydrogenation products. During initial contact with 2-butanol reactants (<600 s) at 373 K, very small amounts (<0.1%) of an organic molecule with a similar boiling point to 2-butanol were detected by gas chromatography. The approximate amount of this product formed during the first 600 s of reaction agrees with the number of Brønsted acid or reduced sites measured on WO_x–ZrO_2 under reaction conditions (Table 5). The exact identity of the by-product formed during reduction could not be determined; but identification based on chromatographic elution times suggests that it is an isomer of 3-butene-2-ol (and not methyl-ethyl-ketone), which can lead to the formation of H-atoms (Scheme 3).

WO_x–ZrO_2 catalysts with intermediate WO_x surface densities stabilize these reduced centers most effectively, because they provide an optimum compromise between WO_x reducibility, which increases with domain size, and W-atom accessibility, which decreases as larger three-dimentional clusters form. Polytungstate domains can successfully delocalize electron density from H-atoms to form $H^{\delta+}$ sites with a density of 0.036–0.040 $H^{\delta+}$/W-atom (Table 5). As WO_x domains oligomerize to form three-dimensional WO_x clusters, the density of these acidic OH groups decreases as they are removed via condensation reactions to form oxygen-deficient WO_{3-x}. These WO_{3-x} structures lead to the broad absorption features observed at high WO_x surface densities in the pre-edge UV–vis region (Fig. 11, W_{30}Z-9.6 and W_{30}Z-17.2). The higher electron density in these oxygen-deficient W species (relative to WO_3) limits their ability to further delocalize the electron density required for the formation of $H^{\delta+}$ sites from 2-butanol. As a result, both the integrated absorption area for W_{30}Z-17.2 and the Brønsted acid site density are lower than those for samples with near-monolayer WO_x surface densities (Table 5). We note, however, that the UV–vis absorption area for W_{30}Z-17.2 is still relatively high in relation to its 2-butanol dehydration rate (Fig. 12), because this area also includes broad background contributions from reduction processes involving oxygen removal, which do not lead to catalytically active $H^{\delta+}$ $(WO_3)_n^{\delta-}$ sites.

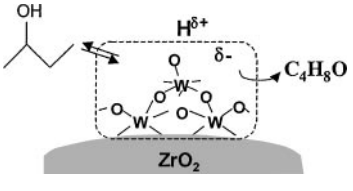

SCHEME 3. Proposed mechanism for the formation of Brønsted acid sites on polytungstate domains in WO_x–ZrO_2. 2-Butanol is activated via dehydrogenation to form H-atoms, which reduce WO_x domains to form $H^{\delta+}$ active sites stabilized over many W-atoms.

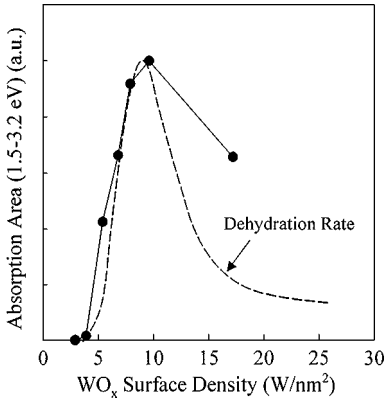

FIG. 12. Integrated UV–vis absorption area (corresponding to the data presented in Fig. 11) as a function of WO_x surface density.

CONCLUSIONS

Acid sites in WO_x–ZrO_2 catalysts with a wide range of surface density were characterized using initial 2-butanol dehydration rates, Brønsted acid site densities measured by titration with 2,6-di-*tert*-butyl-pyridine during reaction, and measurements of localized $W^{(6-\delta)+}$ centers formed during reaction with 2-butanol and observed by UV–vis spectroscopy. Brønsted acid sites are required for 2-butanol dehydration on WO_x–ZrO_2. These active sites form via redox processes using 2-butanol as the stoichiometric reductant to form catalytically active $H^{\delta+}(WO_3)_n^{\delta-}$ sites on polytungstate domains, which can stabilized electron density over several W-atoms without over-reduction. Turnover rates are much higher on these Brønsted acid sites in WO_x–ZrO_2 than on Lewis acid sites in γ-Al_2O_3. The lower acid strength of supported 12-tungstophosphoric acid (HPW) relative to monolayer WO_x–ZrO_2 leads to higher dehydration rates, because of higher rates of product desorption from the weaker acid sites. A proposed mechanism-based kinetic model for 2-butanol dehydration on Brønsted acid sites is consistent with this proposal.

ACKNOWLEDGMENTS

We thank Dr. Stuart L. Soled of the Corporate Research Strategic Laboratory at ExxonMobil for the alumina and the supported tungstophosphoric acid samples. This work was funded in part by the National Science Foundation (CTS-9510575). We also thank Varian for the donation of the UV–visible spectrophotometer used in this study.

REFERENCES

1. Hino, M., and Arata, K., *J. Chem. Soc. Chem. Commun.* 1259 (1987).
2. Scheithauer, M., Grasselli, R. K., and Knozinger, H., *Langmuir* **14**, 3019 (1998).
3. Barton, D. G., Shtein, M., Wilson, R. D., Soled, S. L., and Iglesia, E., *J. Phys. Chem. B* **103**, 630 (1999).
4. Barton, D. G., Soled, S. L., Meitzner, G. D., Fuentes, G. A., and Iglesia, E., *J. Catal.* **181**, 52 (1999).
5. Baertsch, C. D., Soled, S. L., and Iglesia, E., *J. Phys. Chem. B* **105**, 1320 (2001).
6. Wilson, R. D., Barton, D. G., Baertsch, C. D., and Iglesia, E., *J. Catal.* **194**, 175 (2000).
7. Baertsch, C. D., Wilson, R. D., Barton, D. G., Soled, S. L., and Iglesia, E., *Stud. Surf. Sci. Catal.* **130**, 3225 (2000).
8. Kuba, S., Heydorn, P. C., Grasselli, R. K., Gates, B. C., Che, M., and Knozinger, H., *Phy. Chem. Chem. Phys.* **3**, 146 (2000).
9. Iglesia, E., Barton, D. G., Soled, S. L., Miseo, S., Baumgartner, J. E., Gates, W. E., Fuentes, G. A., and Meitzner, G. D., *Stud. Surf. Sci. Catal.* **101**, 533 (1996).
10. Grunert, W., Shpiro, E. S., Feldhaus, R., Anders, K., Antoshin, G. V., and Minachev, K. M., *J. Catal.* **107**, 522 (1987).
11. Larsen, G., Raghavan, S., Marquez, M., and Lotero, E., *Catal. Lett.* **37**, 57 (1996).
12. Boyse, R. A., and Ko, E. I., *J. Catal.* **171**, 191 (1997).
13. Scheithauer, M., Cheung, T.-K., Jentoft, R. E., Grasselli, R. K., Gates, B. C., and Knozinger, H., *J. Catal.* **180**, 1 (1998).
14. Santiesteban, J. G., Vartuli, J. C., Han, S., Bastian, R. D., and Chang, C. D., *J. Catal.* **168**, 431 (1997).
15. Barton, D. G., Soled, S. L., and Iglesia, E., *Top. Catal.* **6**, 87 (1998).
16. Knozinger, H., and Kohne, R., *J. Catal.* **5**, 264 (1966).
17. Knozinger, H., Buhl, H., and Kochloefl, K., *J. Catal.* **24**, 57 (1972).
18. Larsen, G., and Petkovic, L. M., *Appl. Catal. A* **148**, 155 (1996).
19. Kilpatrick, J. E., Prosen, E. J., Pitzer, K. S., and Rossini, F. D., *J. Res. Natl. Bur. Stand.* **36**, 581 (1946).
20. Larsen, G., Lotero, E., Petkovic, L. M., and Shobe, D. S., *J. Catal.* **169**, 67 (1997).
21. Davis, B. H., *J. Catal.* **55**, 158 (1978).
22. Berteau, P., and Delmon, B., *Appl. Catal.* **70**, 307 (1991).
23. Knozinger, H., and Scheglila, A., *J. Catal.* **17**, 252 (1970).
24. Knozinger, H., and Dautzenberg, D., *J. Catal.* **33**, 142 (1974).
25. Noller, H., and Kladnig, W., *Catal. Rev.* **13**, 149 (1976).
26. Hattori, H., and Shishido, T., *Catal. Surv. Jpn.* **1**, 205 (1997).
27. Baba, T., Watanabe, H., and Ono, Y., *J. Phys. Chem.* **87**, 2406 (1983).
28. Sabatier, P., "Catalysis in Organic Chemistry." Van Nostrand, New York, 1923.
29. Soled, S. L., McVicker, G. B., Murrell, L. L., Sherman, L. G., Dispenziere, N. C., Hsu, S. L., and Waldman, D., *J. Catal.* **111**, 286 (1988).
30. Coelho, M. A., Rasasco, D. E., Sikabwe, E. C., and White, R. L., *Catal. Lett.* **32**, 263 (1995).
31. Adeeva, V., de Haan, J. W., Janchen, J., Lei, G. D., Schunemann, V., van de Ven, L. J. M., Sachtler, W. M. H., and van Santen, R. A., *J. Catal.* **151**, 364 (1995).
32. Henglein, A., *Phys. Chem.* **99**, 903 (1995).
33. Alivisatos, A. P., *J. Phys. Chem.* **100**, 13226 (1996).
34. Kettle, S. F. A., "Physical Inorganic Chemistry: A Coordination Chemistry Approach." Oxford University Press, New York, 1998.
35. Kikutani, Y., *J. Mol. Catal. A* **142**, 265 (1999).
36. Kikutani, Y., *J. Mol. Catal. A* **142**, 247 (1999).